IOP Publishing Measurement Science and Technology
Meas. Sci. Technol. **24** (2013) 000000 (17pp) UNCORRECTED PROOF

TOPICAL REVIEW

Advanced giant magnetoresistance technology for measurement applications

Roland Weiss[1], **Roland Mattheis**[2] **and Günter Reiss**[3]

[1] Siemens AG, Corporate Research and Technology, 91058 Erlangen, Guenther-Scharowsky-Str. 1, Germany
[2] Institute for Photonic Technology (IPHT), A.-Einstein-Str. 9, 07745 Jena, Germany
[3] Bielefeld University, Thin Films and Nanostructures, P.O. Box 100 131, 55301 Bielefeld, Germany

E-mail: rolandweiss@siemens.com, roland.mattheis@ipht-jena.de and guenter.reiss@uni-bielefeld.de

Received 28 February 2013, in final form 24 May 2013
Published DD MM 2013
Online at stacks.iop.org/MST/24/000000

Abstract
Giant magnetoresistance (GMR) sensors are considered one of the first real applications of nanotechnology. They consist of nm-thick layered structures where ferromagnetic metals are sandwiched by nonmagnetic metals. Such multilayered films produce a large change in resistance (typically 10 to 20%) when subjected to a magnetic field, compared with a maximum change of a few percent for other types of magnetic sensors. This technology has been intensively used in read heads for hard disk drives and now increasingly finds applications due to the high sensitivity and signal-to-noise ratio. Additionally these sensors are compatible with miniaturization and thus offer a high spatial resolution combined with a frequency range up to the 100 MHz regime and simple electronic conditioning. In this review, we first discuss the basics of the underlying magnetoresistance effects in layered structures and then present three prominent examples for future applications: in the field of current sensing the new GMR sensors offer high bandwidth and good accuracy in a space-saving open loop measurement configuration. In rotating systems they can be used for multiturn angle measurements, and in biotechnology the detection of magnetic particles enables the quantitative measurement of biomolecule concentrations.

Keywords: GMR effect, electron spin, spin valve, multilayer, current sensor, hysteresis modeling, spline interpolation, nanowires, domain wall motion, magnetic storage, biosensor, magnetic marker, single molecule detection, TMR sensors

Q1 (Some figures may appear in colour only in the online journal)

1. Introduction

Q2 Magnetoresistive (MR) effects represent basically the change of a metal system's electric resistivity under the influence of an external magnetic field. There are many configurations possible, depending on the materials used, the functioning principle and the intensity of the effect.

The history of magnetoresistance starts with the discovery of the AMR effect (anisotropic magnetoresistance) in 1856 by William Thomson (Lord Kelvin) [1]. In his reported findings, William Thomson had worked on different samples of iron, nickel, and brass to determine to what extent their conduction would be affected when in the presence of different orientations of a magnetic field. He found no observable results from the piece of brass, however he did find that there was a marked increase in resistance in the presence a magnetic field in parallel to the conductor and a reduction of resistance if the field is perpendicular to the conductor for the samples of iron and nickel. This established the groundwork for magnetoresistance. The one shortcoming to this initial insight would be that it achieves a small effect in low fields, 2% resistance change at room temperature [2]. Due to this,

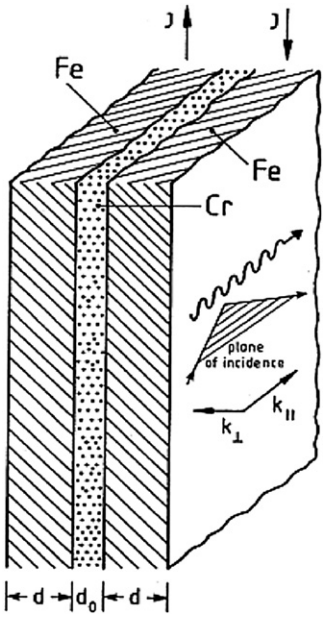

Figure 1. Sketch of the layer system first used to investigate the GMR effect [3].

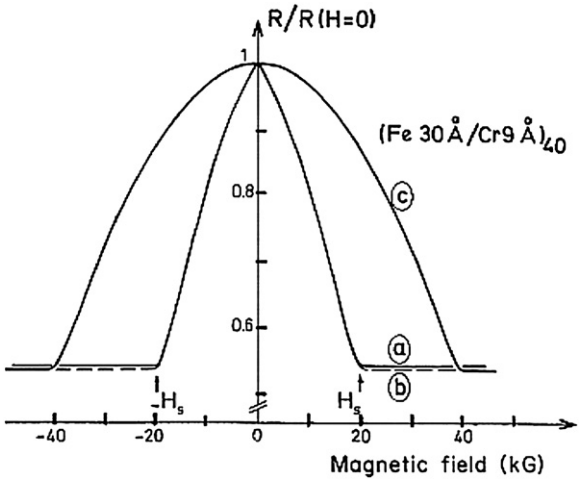

Figure 2. Measurement results for the GMR-effect obtained at 4 K by Fert *et al* [4].

research efforts would not be largely devoted towards the area of magnetoresistance until a hundred years later. The rising demand in magnetic data storage systems starting in the early 70s raised research activities in the fields of magnetic sensing as well. In 1988, Grünberg [3] and Fert [4], with their respective teams in independent discoveries, would break ground on giant magnetoresistance (GMR). Pushing the front on William Thomson's earlier work, their findings showed that it was possible to generate changes in resistances on a greater scale than had been thought possible. This result was possible through the stacking of Fe/Cr/Fe layers as shown in figure 1, which demonstrated resistance changes outwards of 10% to 50% as shown in figure 2. Their remarkable findings were rewarded with the presentation of the Nobel Prize in Physics in 2007 [5]. As momentous as the discovery was, it still presented two major hurdles for being implemented in an industrialized production setting. First of all, their experimental samples involved a careful, complex production method known as molecular beam epitaxy, a method of depositing single crystals that creates a uniform film of a substance on a target surface. This form of production did not lend itself towards simple adoption at the time within a large-scale production setting. Second, their experiments demonstrated their best results at low temperatures (50% at 4 K and 10% at 5 K by the teams of Fert and Grünberg, respectively), although Fert did report that significant MR effects were still present at room temperature.

Understanding the inherent potential in GMR, Parkin and his colleagues working within IBM Almaden Research Center opted to experiment on whether sputtering—a common hard drive manufacturing technique at the time—could be adapted so as to manufacture devices that could take up the properties demonstrated by Grünberg and Fert without the complex method of material layering they had used in creating their samples. Sputtering involves bombarding the surface of a target material to knock off atoms and to deposit those atoms on the samples surface, thus creating a very thin layer of the target material on the sample. Parkin and his team found their work to be successful [6], leading to an ever since increasing storage density in hard drives. The commercial success stimulated research in MR-effects and so besides AMR and GMR a lot of other MR-effects such as TMR (tunneling magnetoresistance), CMR (colossal magnetoresistance), GMI (giant magnetoimpedance) or OMR (organic magnetoresistance) had been discovered. Moreover, applied research, improved quality and reduced cost of GMR-technology open further applications in the field of position sensing, biomagnetism, MRAM (magnetic random access memory) and current sensing. The first automotive sensor appeared in 1993 more than four years before the first GMR read head sensor for the hard disk was introduced into the market [7]. MR sensors nowadays have found many applications ranging from the automotive sector to biophysics [8]. In particular for automotive applications, position- and angle-sensors are key-devices and there has been intensive search on this field [9, 10] which cannot be covered completely in one article. In this review we will briefly introduce the basics of the GMR effect and then discuss some specific examples for advances which have been made in the last couple of years on current sensing, sensors with storage functionality and applications of GMR sensors in biotechnology.

2. Fundamentals of GMR technology

Due to the intensive research in magnetism there is a large variety of effects that can be used to measure magnetic properties like the magnitude or direction of the magnetic field strength or the magnetic flux density. Figure 3 gives an overview about different technologies and the magnetic flux density range where the corresponding technology can be used. From this comparison it can be seen that MR effects are usually used to measure small (about 10^{-11} T) up to medium (about 10^{-2} T) magnetic fields.

2.1. Different magnetorestive effects

As so many different magnetic effects are known, each leverages a balance of different advantages and disadvantages in their performance and costs. Since many of these branches of magnetoresistance have had extensive research devoted to each, for brevity the essential characteristics that differentiate GMR from other magnetoresistance technologies and their devices are as follows.

2.1.1. Hall effect. Hall-effect sensors can be easily built with semiconductor equipment and thus also be integrated with high performance analog and digital electronic on the same chip. The combination of Hall-effect sensors on silicon and high performance analog and digital electronic on the same chip shows usually a good performance for standard industrial measurement purposes.

2.1.2. AMR. Anisotropic magnetoresistance, along with GMR, is the most mature of the magnetoresistance developments. Although often found deployed in applications due to lower associated costs, AMR is not able to achieve the same large signal as GMR. But with regard to the sensitivity of AMR sensors, their measurements in mV/(VT) is comparable about 10 000 mV $(VT)^{-1}$ to that of those of GMR sensors and so therefore are much better than Hall elements [12].

2.1.3. TMR. Tunneling magnetoresistance involves the use of an insulating layer rather than a metallic one, found in the GMR sensor to be sandwiched between the ferromagnetic layers and involves the quantum tunneling of electrons through the insulating layer. Although it tends to yield greater resistance changes than GMR, it also suffers from exhibiting generally a larger and highly nonlinear resistance thus mitigating some uses where a low bridge offset voltage and PSRR (power supply rejection ratio) may be required.

2.1.4. SQUIDs. Superconducting quantum interface devices (SQUIDs) boast the highest degree of accuracy and resolution. SQUIDs, however, are constrained to specialized tasks due to its prohibitive costs and the difficulty in its implementation. These are both tied to SQUIDs' requirement that it must be operated at extremely low temperatures in order to work, thus requiring special cooling systems in its construction.

2.1.5. CMR. Colossal magnetoresistance is relatively new compared to the other options. CMR can theoretically achieve massive changes to its observed resistance in varying magnetic field directions [13]. However, it suffers greatly from temperature effects. CMR is also limited by the requirement of sizably large magnetic fields of 1 T [14]. CMR effects of over 200% have been reported.

2.1.6. GMI. In soft ferromagnetic wires or ribbons the ac complex impedance depends on the used frequency and on the applied magnetic field that can be caused by different effects such as the gyromagnetic effect and ferromagnetic relaxation or the skin effect. Phan *et al* reported GMI effect of over 250% [15].

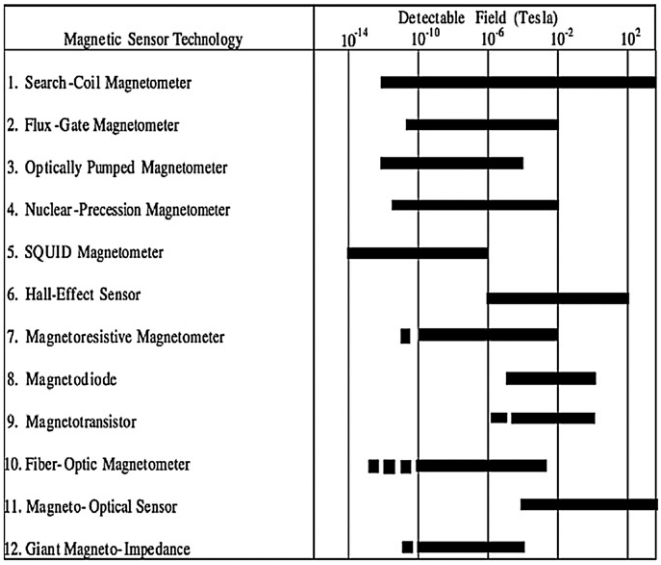

Figure 3. Overview on some of the different technologies to measure magnetic flux density [11].

2.1.7. OMR. Organic magnetoresistance finds itself as a recently discovered MR-type, with the discovery of its effects having been realized as recently as 2004. Composed of an organic semiconducting material, OMR is special in that it generates its MR effect without the use of magnetic materials; experimental research demonstrated a 10% resistance change in a 10 mT field at room temperature [16]. However, like CMR, OMAR is relatively new in its implementation. Also, its mechanism is not completely understood, and no materials or methods are yet known to diminish its high temperature coefficient.

2.2. Spintronics and GMR effect

GMR is observed in structures which exist of alternating ferromagnetic and nonmagnetic layers with a thickness of some tenth to few nanometers. The effect allows altering the electrical resistance of the entire layer structure through a change of the mutual magnetization orientation of the soft magnetic layers. In figure 2 the relationship between the mutual magnetization orientation, the resistance and the magnetization orientation can be seen. If the layers are magnetized in opposite direction, the resistance is for many cases, such as Co/Cu/Co or $Ni_{80}Fe_{20}/Cu/Ni_{80}Fe_{20}$, significantly higher than with magnetization in the same direction. If the spin asymmetry of the resistivity of the magnetic layers has an opposite sign, the resistance can also be lower for antiparallel than for parallel alignment of the magnetizations as demonstrated by Violle *et al* [17].

The reason for that is the spin-dependent scattering and therefore the conductivity of electrons in ferromagnetic materials, which is a well-known quantum mechanical phenomenon first proposed by Mott [18]. Following Mott's proposal, the electrical conductivity in metals can be described by using two largely independent conducting channels, corresponding to the up-spin and down-spin electrons. Due

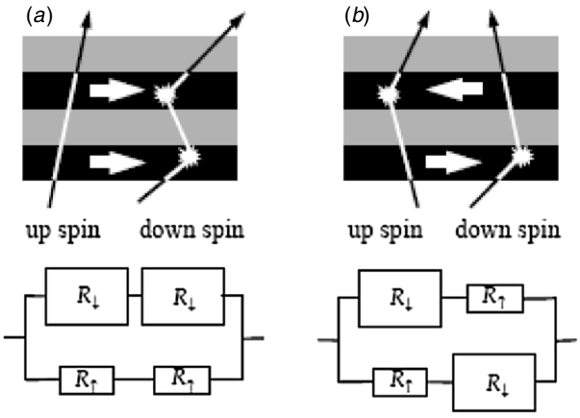

Figure 4. Illustration of electron transport in magnetic multilayer's for parallel (*a*) and antiparallel (*b*) magnetizations [19].

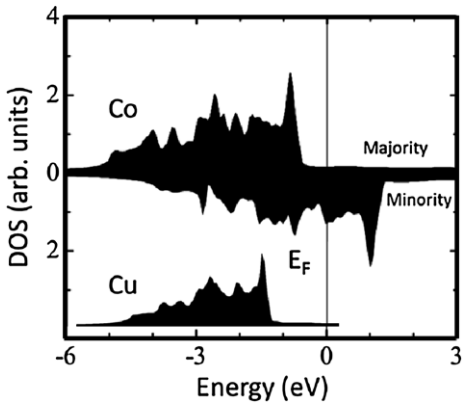

Figure 5. The DOS for the majority and minority electrons of Co and for the electrons of Cu [14].

to the low probability of spin-flip scattering compared to scattering processes, in which the spin is conserved, the up-spin and down-spin electrons do not mix over long distances and so, the electrical conduction occurs like two spin channels (up-spin and down-spin) in parallel as illustrated in figure 4. That so-called two channel model despite being largely simplified can be used to illustrate the GMR-effect.

With the idea of the two channel model from figure 4 and corresponding figure 5, it is straightforward to assume that the total resistance for antiparallel magnetizations of the layers is higher compared to parallel magnetizations of the layers forming the conductor and to calculate the GMR ratio according to [19, 20]:

$$R_{\uparrow\uparrow} = \frac{4(R_\uparrow R_\downarrow)}{2(R_\uparrow + R_\downarrow)} \quad R_{\uparrow\downarrow} = \frac{(R_\uparrow + R_\downarrow)^2}{2(R_\uparrow + R_\downarrow)} \tag{1}$$

$$\mathrm{GMR}(\%)\frac{\Delta R}{R} = \frac{(R_\downarrow - R_\uparrow)^2}{4(R_\uparrow R_\downarrow)}. \tag{2}$$

The microscopic reason for the GMR is mainly the different scattering of the majority and minority charge carriers of the ferromagnet. This results from the electronic band structures and can be explained in a crude approach already by the density of states DOS. For a typical GMR multilayer stack, e.g. Co/Cu/Co, the DOS is illustrated in figure 5.

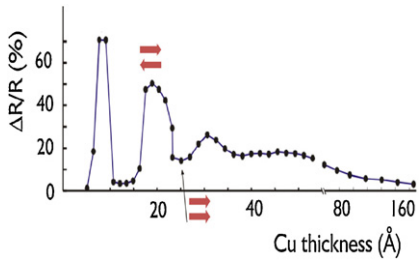

Figure 6. Measurement of the GMR effect in Co/Cu multilayers (polycrystalline) with 2 nm Co thickness as a function of the Cu thickness at 4K [21].

While the nonmagnetic spacer like Cu and the majority electrons of the Co have only a small and flat s-like DOS at the Fermi energy E_F, the minority carriers of the Co have a large DOS of mainly d-type. For other ferromagnets such as Fe, the amount of d-states at E_F can vary considerably. For the Co/Cu/Co system and many others, however, the asymmetry in the majority and minority DOS at E_F gives rise to a strong scattering of the electrons of the nonmagnet and of the minority carriers via the s-d scattering mechanism. In contrast, the s-like states have a low DOS and thus the s-s scattering is weak. In terms of a mean free path l_{mfp}, this implies a very short l_{mfp} for the minority and a long one for the majority electrons in agreement with Mott's two band model.

If one considers a GMR multilayer stack as illustrated in figure 4, the thicknesses t_{FM} and t_{NM} of the ferro- and the nonmagnetic layers also have a strong impact on the magnitude of the GMR. While the GMR usually drops steadily with increasing t_{FM} above a thickness of around 2 nm due to simple shunting effects, the dependence on t_{NM} shows an oscillator behavior as illustrated in figure 6 for Co/Cu/Co. This is due to the oscillation of the magnetic coupling between antiparallel and parallel which can be explained by a confinement of the electrons within the very thin layers. The envelope, however, again shows a steadily decreasing GMR due to shunting.

For sensing applications, the temperature dependence of the GMR amplitude is another very important parameter. While the magnetization of the ferromagnet usually is nearly constant for typical application temperatures, the scattering of the electrons at phonons shortens the mean free paths of the charge carriers and thus an increase in temperature leads to a decrease of the GMR amplitude as shown in figure 7. This decrease, however, is by far weaker as for, e.g., semiconductors and shows a nearly linear behavior around room temperature similar to the resistance itself. Thus compensating the temperature dependence is—although usually necessary—relatively simple for GMR based sensors.

The distinctive relationship between the magnetization orientation of the magnetic layers and the electrical resistance is perfectly applicable for measuring external magnetic fields. The GMR sensor used for measurement purpose usually favors two different layer systems: one is a so-called spin valve system the other is a multilayer system.

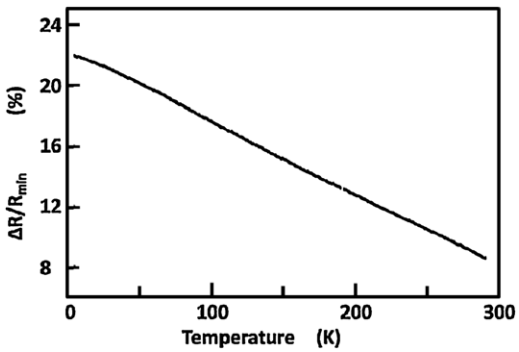

Figure 7. GMR versus temperature for a Co/Cu multilayer with 5 nm Co and 2 nm Cu [22].

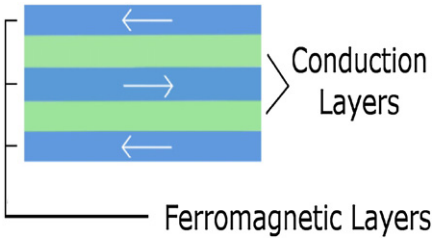

Figure 8. Schematics of a GMR-multilayer sensor without external magnet field.

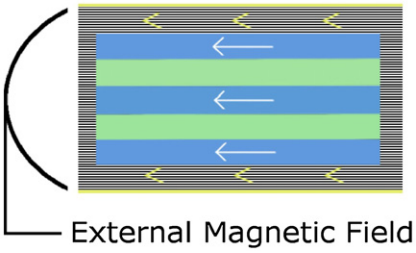

Figure 9. Schematics of a GMR-multilayer sensor with external magnet field.

2.3. Multilayer GMR sensors

Multilayer consists of many alternating layers of ferromagnetic and nonferromagnetic material. By having many layers contributing to the GMR effect, the observed GMR effect is quite large (up to 80% at 4.2 K) [23]. In the absence of an externally applied magnetic field, adjacent layers demonstrate that they have a tendency to align themselves so as to have their own fields be arranged in an antiparallel configuration due to interlayer coupling and stray field coupling for very small structures as sketched in figure 8.

Varying the thickness of the metallic nonmagnetic layers alters the occurrence of antiparallel adjacent layers [24]. Increasing the thickness d_{FM} of the ferromagnetic layer decreases the obtainable DR/R. Nevertheless the sensitivity DR/R/DH increases because the field necessary for achieving parallel alignment as shown in figure 9 scales with $1/d_{FM}$, whereas the DR/R decrease is much weaker than $1/d_{FM}$. One limitation to multilayer GMR is their requirement to be exposed to large fields and the largely nonlinear output characteristic (see figure 2), thus hindering their general use in some electronic devices.

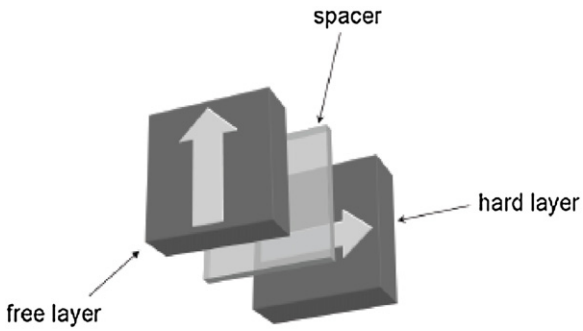

Figure 10. Sketch of a GMR spin valve sensor.

2.4. Spin valve GMR sensors

As shown in figure 10, GMR spin valve sensors basically consist of two ferromagnetic layers, separated by a nonmagnetic metallic layer. One of the ferromagnetic layers acts as a reference system which is built and conditioned to have a fixed magnetization vector (hard layer or reference layer). The other ferromagnetic free layer features a relatively free moving magnetization direction (free layer). The direction of the magnetization vector of the free layer is influenced by the external magnetic field leading to a change in the resistance of the GMR spin valve sensor. Under appropriate conditions the spin valve system shows an approximately linear resistance change of typically 10% and a sensitivity of about 20 mV $(\mathrm{VmT})^{-1}$ and is therefore often favored for measurement purposes like electrical current measurement or linear position measurement.

3. Advances in GMR current sensing

The standard methods for measuring electrical current include mainly Hall sensors, AMR sensors, shunts, or fluxgate detectors. Shunts are very accurate but have the disadvantage of not being electrically isolated from the measured circuit. The other technologies usually have to be used in a power- and space-consuming closed loop system to provide a good bandwidth and a suitable accuracy such as the LEM IT series current sensors. Compared to other technologies, the new GMR-current sensors offer the advantage of high bandwidth and good accuracy in an open loop measurement configuration.

3.1. Physical structure of GMR-current sensors

To exploit the advantages of the high frequency (up to several GHz) and high sensitivity (20 mV $(\mathrm{VmT})^{-1}$) capabilities of GMR sensors, an open loop configuration without flux concentrator is usually used for current measurement as shown in figure 11. According to Ampère's circuital law, the primary current causes a magnetic field H around the conductor it passes through. This conductor is attached to the GMR element with an isolation layer in-between, made of PCB material. As shown in figure 9 the GMR sensors are arranged in a dedicated Wheatstone configuration on a u-shaped conductor to enable differential measurement and are cross connected to work with a uniform reference

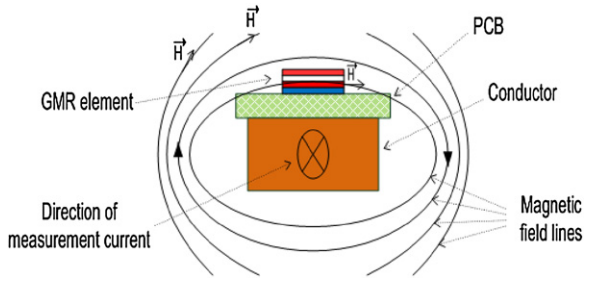

Figure 11. GMR element for current sensing.

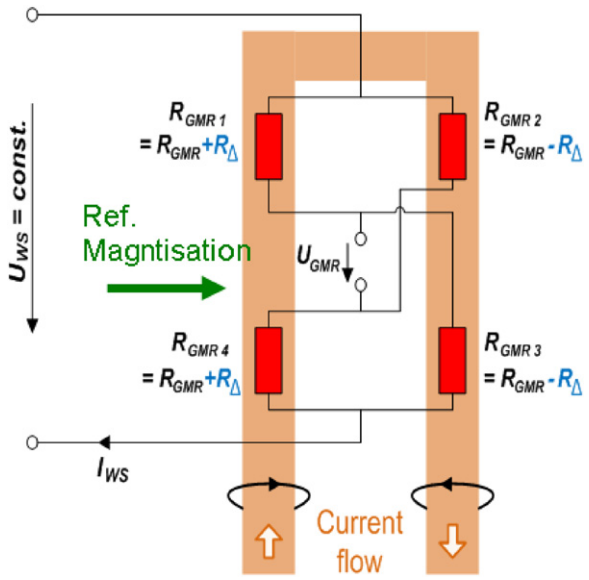

Figure 12. Schematics of a Wheatstone bridge of four GMR elements stimulated by a current-carrying U-shaped conductor.

direction in all four GMR elements. Basically a change of the current in the u-shaped conductor alters the magnetic field, which in turn results in a rotating magnetization of the free layer of the spin valve GMR element. The advantage of the arrangement shown in figure 9 is that the complete bridge with four GMR elements can be made simultaneously on the same chip. This usually increases the uniformity of the four GMR elements significantly. The high uniformity will result in low offset errors and improved linearity. In addition to the u-shaped conductor shown in figure 12, meander-shaped conductors have also been investigated by Beltran *et al* [25]. The meander-shaped conductors also show the benefit that all four GMR elements can be made simultaneously on the same chip [26]. The principle drawback of the meander-shaped conductor is the large GMR-chip size for measuring larger electrical currents which has not been solved yet. Both the meander-shaped and u-shaped conductor-based arrangements compensate foreign magnetic fields with identical impact on all GMR elements and even temperature influence to some extent. Due to the fact that only magnetic fields with identical impact on all GMR elements are compensated, there is in principle an influence from inhomogeneous external magnetic field on the sensor. To keep that influence small, usually the distance between both sides of the Wheatstone bridge should be kept small as well.

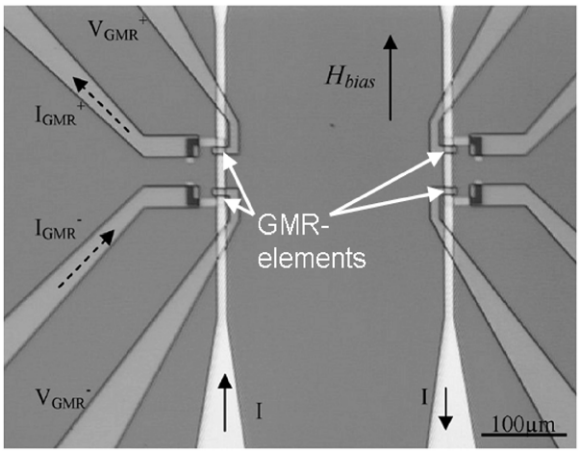

Figure 13. Picture of a GMR-current sensor for currents up to 100 mA [27].

Another drawback from the configuration shown in figures 11 and 12 is that the sensitivity of the sensor depends on the distance between the sensor and the conductor; therefore usually a high-quality mounting for the sensor on the conductor has to be used to limit the corresponding error, due to aging and mechanical stress, to 0.1%.

To keep the effort for circuitry low, usually such a Wheatstone bridge consisting of four GMR resistors is supplied with a constant voltage ranging from 3.3 to ±12 V. As output, a single voltage signal U_{GMR} is provided, which equals ideally zero when no current flows.

In that way, GMR sensors can be used for precise current measurement in the range from mA to several 100 A without bulky flux concentrators or sophisticated and power-consuming 'closed loop' circuits, i.e. analog circuits, giving them a clear advantage over current measurement systems exploiting the Hall effect.

3.2. GMR-current sensors without signal conditioning

The first approaches for current sensing with GMR sensors only used the small output signals of Wheatstone bridges consisting of four GMR elements of the spin valve type to determine the current. Those first comparable cheap and small current sensors have mainly been investigated and used for measuring currents in the mA range by keeping a galvanic isolation to the current measured. The sensors for measuring small currents used a chip integrated current conductor as shown in figure 13 [27]. According to Pannetier–Lecoeur *et al* [27] the GMR sensor they investigated was able to measure currents up to 100 mA. For larger currents an integrated line with a larger width than the GMR could be used. They also found for the GMR-sensors, which consisted of Ta 5 nm/$Ni_{81}Fe_{19}$ 3.5 nm/$Co_{90}Fe_{10}$ 1.2 nm/Cu 2.1 nm/$Co_{90}Fe_{10}$ 2.5 nm/IrMn 10 nm/Ta 10 nm and had been deposited by sputtering on a silicon substrate, a noise that is typically 10–100 nV $Hz^{-1/2}$ at low frequencies ($1/f$ noise of the sensor).

An example of a commercially available current sensor measuring in the mA range is the NVE AAV003-10E sensor.

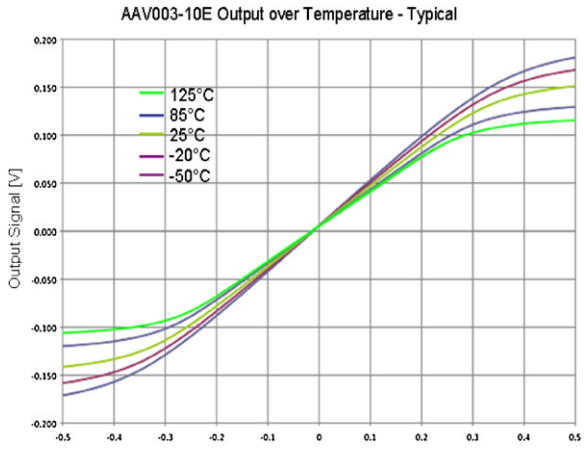

Figure 14. Output characteristic of a NVE AAV003-10E GMR-current sensor [28].

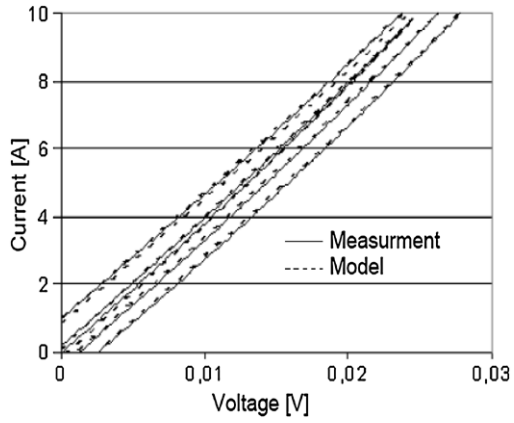

Figure 15. Comparison between the real-time calculated hysteresis loops including major and minor loops (model solid line) and the directly measured hysteresis loops (dashed line).

The output characteristic of the Wheatstone bridges consisting of four GMR elements (spin valve type) is shown in figure 1. The output characteristic indicates an offset error range of about $\pm 4\,\mathrm{mV\,V^{-1}}$ and a temperature coefficient ($-0.17\%/^{\circ}\mathrm{C}$) of the sensors output voltage.

To overcome those and other errors, research for adapting the GMR sensor for high accuracy current measurements is still going on.

One approach is an improved design of the GMR element which resulted in an improved temperature characteristic of the output voltage as shown in figure 18 (temperature coefficient of about $0.08\%/^{\circ}\mathrm{C}$). Besides that, digital electronic circuits have been developed to increase the accuracy of GMR technology based current sensors.

3.3. GMR-current sensors with signal conditioning

There are two promising methods for compensating different errors such as offset, nonlinearity, hysteresis and temperature drift of GMR Wheatstone bridges. If the dominant error is caused by magnetic hysteresis, modeling of the hysteresis as shown in the next section is up to now the most promising method. In other cases, special interpolation methods like B-spline interpolation were successfully applied.

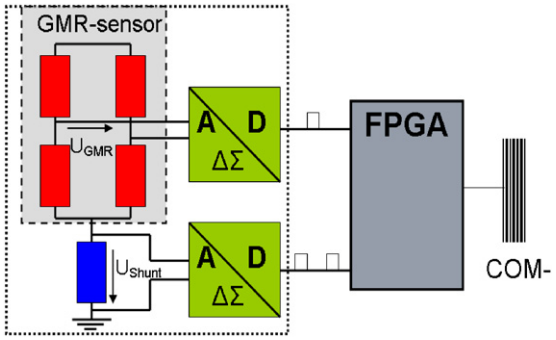

Figure 16. Schematics of a GMR sensor system for a single current.

3.3.1. Hysteresis modeling. A quite successful method described by Jedlizca *et al* was the real-time modeling of the hysteresis loop of a GMR-current sensor [29]. A simple analog circuit for amplification and a low-pass filtering in combination with a DSP (digital signal processor) of medium performance were used for the real-time correction of all nonlinearities including hysteresis with a special polynomial model. The result was a reduction of the total measurement error from 2.87% to 0.74% at a defined temperature [30]. After a first magnetic field pulse—to set the sensor into a defined state in the saturation area of the 'major loop'—the electronic system followed in real-time mode the inverse 'minor loop' and calculated the current from output voltage of the GMR Wheatstone bridge. The calculeted current showed a largely reduced error compared to the current directly gained from the output voltage of the GMR Wheatstone bridge as has already been metioned. Figure 15 shows the comparison between the calculated current values and the measured reference current values over several cycles of triangular current pattern. One drawback of this method found by Jedlizca *et al* was the difficulty to compensate the effect of fast changing temperatures on the output signal, due to the limits of the hysteresis model [30].

3.3.2. B-spline interpolation. Another method to improve the accuracy of GMR-current sensors with digital signal conditioning is the two-dimensional B-spline interpolation which was presented by Bluemm *et al*. Their method used the voltage drop over a simple shunt resistor, which was connected in series with the Wheatstone bridge (see figure 16) and allowed the measurement of the temperature of the GMR elements [31]. With the information about the temperature, digital signal correction is improved remarkably, as will be shown later.

A shunt resistor was useful since the total bridge resistance R_{WS}, and therefore the feeding current I_{WS}, depends directly on the temperature of the GMR-elements. On the other hand, R_{WS} and I_{WS} are independent of the stimulating magnetic field, due to the special arrangement of the GMR elements.

Consequently the Wheatstone/shunt combination provides two independent output signals: U_{GMR} represents the external magnetic field and U_{shunt} represents the temperature. As soon as these signals are digitalized, they can be conditioned with the FPGA. In the sensor system presented here,

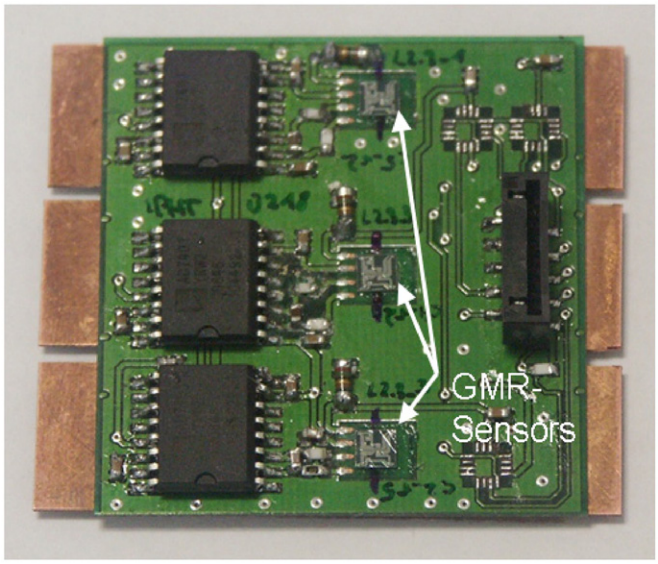

Figure 17. Picture of a current sensor system for measuring three different currents (developed by Siemens).

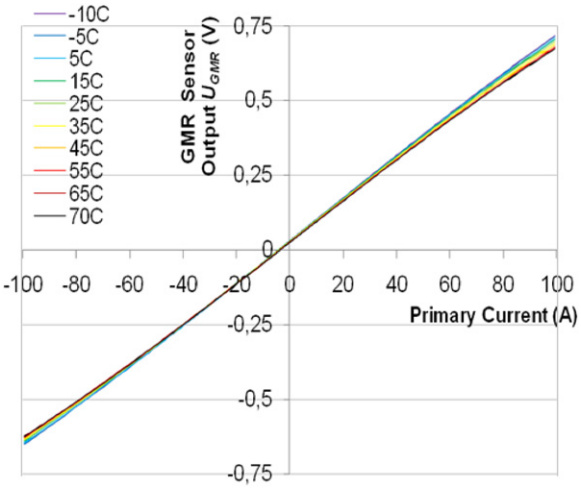

Figure 18. Measurement of a typical analog input–output interrelation of a GMR Wheatstone bridge used for current sensor.

the $\Delta\Sigma$ modulators AD7401 from Analog Devices are used for digitalization.

Additionally, the original Siemens sensor system presented by Bluemm *et al* can handle three-phase instead of one-phase currents. Thus, all circuit elements of figure 16 are tripled, except for the FPGA. A picture of such a three-phase GMR-current sensor system is shown in figure 17.

For digital signal conditioning, an adaptation of the B-spline interpolation method and a look-up table was used to correct the influence of nonlinearities and the temperature on the measured current value.

Typical uncorrected output voltage values of the GMR-Wheatstone bridge are presented in figure 18. Therefore, dc currents in the range of $\pm$ 100 A at temperatures from -10 °C to 70 °C are applied to stimulate the GMR technology based sensor. Compared to the output characteristic of other current sensing elements, shown in figure 14, the sensor

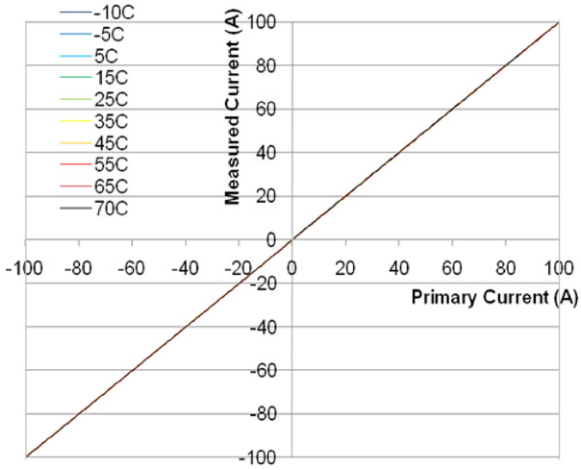

Figure 19. Output characteristic of the digital GMR-current sensor with linearization by B-spline interpolation.

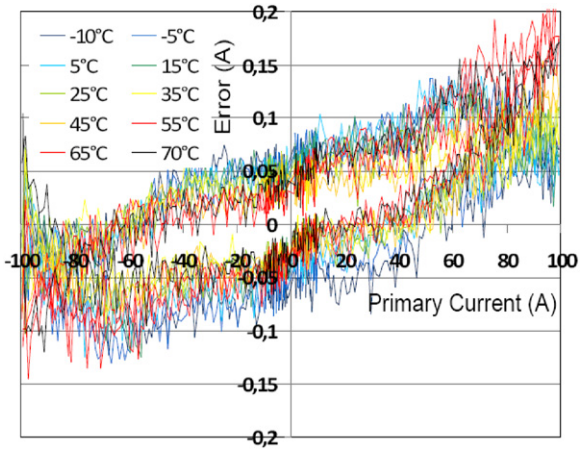

Figure 20. Evaluation results for the absolute error of the linearized measurement.

characteristic was already considerable. Yet, there is still room for digital improvement. With the B-spline interpolation method described in [31] a linear output characteristic was obtained (see figure 19) resulting in a total error of 0.25% in a temperature range from -10 °C to 70 °C (see figure 20).

For a quantitative evaluation, figure 20 gives the corresponding absolute measurement error. All measurement operations were run from the minimal to the maximal current value and back. In doing so, the hysteresis behavior of the GMR sensor shows its ultimate occurrence [32], clearly noticeable in figure 20. This means that the resulting error plots gives the worst-case scenario for the error. In real measurements, however, less hysteresis impact can be expected and therefore a higher accuracy can be obtained.

4. GMR sensor with storage functionality: multiturn counter

For sensors where a linear response is required, such as current sensor, angle detection sensor, compass or hard disk read heads, a nearly vanishing hysteresis is mandatory. Vanishing

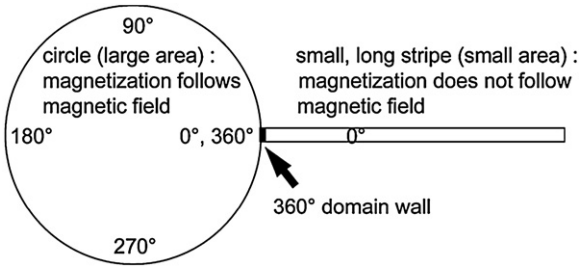

Figure 21. Domain wall generator as a disk with a diameter of the order of 10 μm, connected with a GMR nanowire, line width of the order of 200 nm, thickness of the sensor layer ~20 nm, from [33].

hysteresis can be achieved by using geometry (layout) where the remagnetization process is characterized by pure rotation of the magnetization avoiding any process connected with domain generation and domain wall motion. Nevertheless some large-scale applications demand an additional counting functionality, i.e. the angle detection range has to be expanded up to n turns ($n \times 360°$). In applications like sensing of steering wheel position the angle range has to be extended to five full turns. Other applications need maximum turn number ranging from ten (10 turn potentiometer) to thousands of turns, e.g. for motor feedback systems for industrial applications. Another potential large-scale application is the measurement of one full turn with higher resolution by using a magnetic pool wheel with n north and south poles. In combination with a magnetic angle sensor an accuracy improvement can be achieved getting $1/n$ of the original accuracy at much less sensor costs as compared to high resolution optical sensors.

4.1. Principle of domain wall based sensing

Having in mind the remagnetization route of a pure Stoner–Wohlfarth particle, it behaves like a permanent magnet as long as the field acting to this particle is lower than half of the so-called anisotropy field strength H_k. In the layout under discussion (see figure 21) H_k is determined by the geometry of the structures because the intrinsic anisotropy field for $Ni_{81}Fe_{19}$ thin films is of the order of 250–300 A m^{-1}, much below the shape anisotropy of the used nanowires. This allows constructing a magnetic conduit system allowing for generation and storage of magnetic domain walls by selecting the right geometry. A circularly shaped $Ni_{81}Fe_{19}$ disk exhibits a vanishing in-plane shape anisotropy for a nearly hysteresis-free rotation of the magnetization within this part as long as the magnetic field strength is sufficiently larger than the anisotropy field caused by the deposition-induced anisotropy field strength H_k^{ini}, which is of the order of 200–300 A m^{-1}.

In a GMR nanowire the shape anisotropy H_k scales with d/w times Ms with d thickness of the magnetic layer acting as the conduit of the domain walls (here the typically thick 20 nm $Ni_{81}Fe_{19}$) and w width of the nanowire, length $\gg w$, and M_s saturation magnetization. For a 200 nm wide GMR stack we obtain H_k values of about 75 kA m^{-1}, 300 times the value of H_k^{ini}.

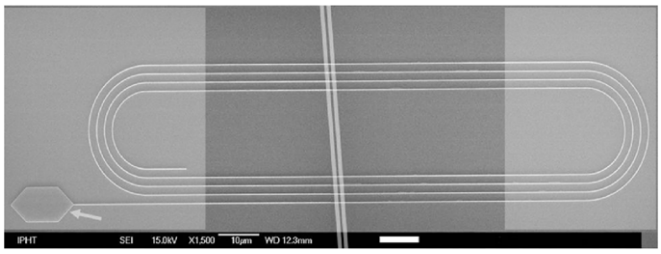

Figure 22. Composed picture of two SEM micrographs, showing the right and the left part of a multiturn counter with four turns. The middle part of the straight stripes with a length of approximately 380 μm is cut out. Al contact pads covering the curved regions of the spiral are seen as overlaid bright gray areas. They are used as electrical contacts. The arrow (lower left) is directed to the enlarged area responsible for the generation of the domain walls.

4.2. Race track-like multiturn

A first proposal to use the generation and storage of 360° domain walls in structures was presented in 2004 adapted from figure 1D of [33]. This idea was extended to a spiral-like geometry by Geng *et al* [34]. The promising results obtained by micromagnetic simulations, namely the storage of ten 360° domain walls in the proposed structure [33], could not be sufficiently verified in experiments. The reason is probably connected with interactions of the individual 180° domain walls leading to annihilation or expansion. To avoid these interactions a changed geometry was checked allowing for an individual handling of every 180° domain wall [35]. By combining a domain wall generator with a nanowire forming a race track-like geometry as shown in figure 22 every half turn of the rotating magnetic field generates a 180° domain wall. This wall was transported a half turn inside the spiral for the case the sense of the spiral corresponds to the sense of the rotating field before the next 180° domain wall was generated in the domain wall generator. This guarantees a continuous flow of 180° domain walls with no interaction between them. By changing the sense of the rotating magnetic field all the 180° domain walls located inside the race track are transported in the direction of the domain wall generator and are annihilated by the domains which are generated inside the domain wall generator. Q4

The counting of a low number of turns (<10) can be done by reading the resistance of the whole race track as shown in figure 2D. A GMR stack (seed layer/7IrMn/2.5$Co_{90}Fe_{10}$/0.8Ru/2.5$Co_{90}Fe_{10}$/2/0.8$Co_{90}Fe_{10}$/20$Ni_{81}Fe_{19}$/5TaN, all values in nm) is patterned and the reference direction is parallel to the race track. As shown in [35] up to 10 separated resistance values can be recognized. Q5

To suppress the effects caused by the temperature coefficient of the resistance, a Wheatstone bridge configuration has to be created. By using race tracks with clockwise and counter clockwise sense as parts of a Wheatstone bridge a suppression of the temperature coefficient T_k can be achieved. The inherent hysteresis of the domain wall motion can be overcome by using two structures rotated by 180° against each other.

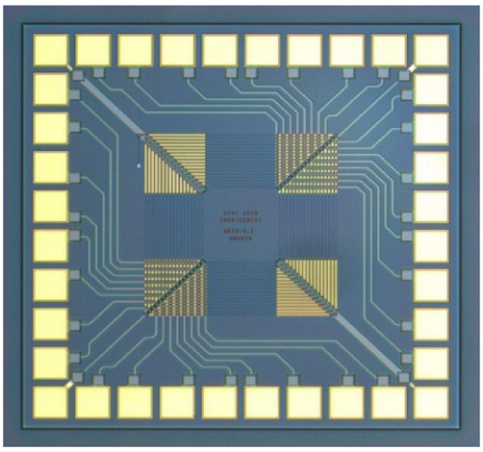

Figure 23. Chip layout of the today's multiturn sensor used in the Novotechnik system Multiturn sensor type RSM 2800.

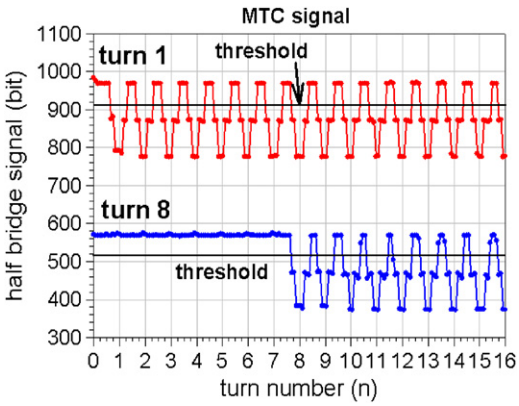

Figure 24. Wheatstone half bridge signal at of the first and eight turn output in dependence of the number of rotations, for clearance the signals are shifted by 400 bits.

4.3. Quad16 multiturn

To overcome the limitation of the race track like multiturn (maximum number of turns $N < 10$) the read-out scheme has to be changed. Figure 23 shows the die of a commercially available counter for counting of up to 16 turns. Here the domain wall generator is connected to a spiral with nearly quadratic shape. By directing the reference direction in one of the two diagonals and connecting every individual half turn we get an individual signal which is independent of the number of turns of the spiral. An example of the dependence of the individual bridge signals for the first and eight full turn is shown in figure 24. Here a constant signal indicates no domain wall within the turn. Details of the of the signals' curvature are discussed in [364]. The price we have to pay for this turn number-independent signal is the large number of read-out pads. Standard circuiting needs two pads for V_{cc} and gnd, and $2N$ pads for the N turn spiral. By multiplexing the number of pads it can be reduced to $4\sqrt{N}$ for N equal power of 2. That means for $N = 16$ we need 16 contacts instead of 34 for standard circuiting and for $N = 64$ 32 contact pads are necessary for a complete read-out. $N = 64$ seems to be the maximum for that kind of a GMR sensor type because the

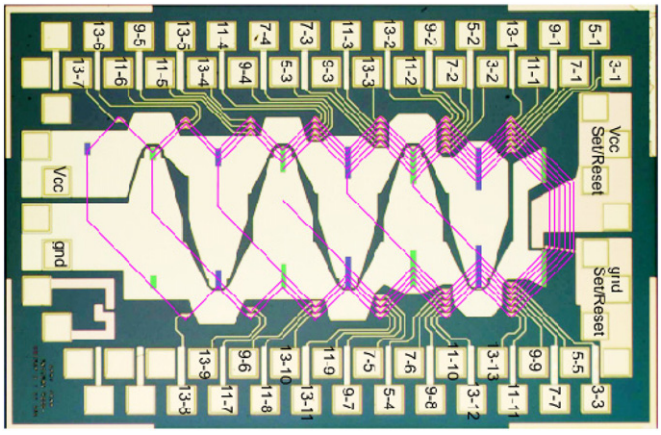

Figure 25. Chip layout of a sensor using six loops for $N = 3, 5, 7, 9, 11$ and 13 turns.

increasing length of the spiral causes problems with the yield. At least a length in the order of about $l = 100$ μm should be available between the contact areas for an easy read-out of the resistance. This causes a spiral length of $4N^*l$, where $N = 16$ is a lower limit of the spiral length of 6.4 mm, and 25.6 mm for $N = 64$. By using a distance from turn-to-turn of $a = 2$ μm, it causes an additional length of $2N^2a$, e.g. 1 mm for $N = 16$ and 16.4 mm for $N = 64$. This length could be drastically reduced by using a TMR stack. Then the characteristic length can shrink from 100 to 10 μm or less. In that case the factor $2N^2a$ determines the total length. But N values above 128 are clearly excluded with this spiral solution.

4.4. Closed loop counters

Larger number of turns or application within a pole wheel is needed for a new domain wall based design. A possible solution is the joint use of different closed loops as proposed in [37] and shown in figure 25. Here by using loops each loop is able to count a number of turns which is prime to the number of all the other loops, the whole system is able to count the product of the numbers of all loops, e.g. by using loops which are able to count 5, 7, 9 and 11 turns by themselves the combination results in a system of loops able to count to $5^*7^*11^*13 = 5005$ number of turns. In the pointed solution [37] the individual loops use cusps proposed by Allwood *et al* [38, 39] for the construction of a magnetic NOT gate. A 180° domain wall needs a 180° rotation of the rotating magnetic field to move through a cusp. Therefore a domain wall located in a closed loop with n cusps directed to the inner part of the loop needs $n + 2$ half turn rotation of the magnetic field to achieve the starting position. From topological reasons a loop with even number n ($n = 2c$) of cusps contains an even number of domain walls namely from 0 in steps of 2 to a maximum number of $2n + 2$. In contradiction, a loop with an odd number n ($n = 2c + 1$) of cusps contains an odd number of domain walls, at least one and in maximum $2n + 1$ domain walls.

The transition of one or an odd number of domain walls at any arbitrary position of the loop ends up with a state at this position where the magnetization direction is reversed after this transition as compared to the initial situation. Therefore

we need a twofold transition of every domain wall in a system $n = 2c + 1$ to end up not only with the state every domain wall reaches its starting position but also with the starting configuration of the magnetization. To illustrate this let us consider four loops with odd numbers of cusps, namely 3, 5, 7 and 11. An individual domain wall reaches its starting position after 5, 7, 9 and 13 half turns. The starting magnetization configuration is independent of the concrete starting state achieved after 3, 5, 7 and 11 full turns. Therefore by using a proper starting configuration, in the simplest case every loop filled with exactly one domain wall, every configuration of magnetization repeats after 3*5*7*11 = 1155 turns.

The use of a number of closed loops offers the advantage of achieving a large number of countable turns, e.g. the eight loops 5, 7, 9, 11, 13, 17, 19 and 23 allow for counting of ∼330 Mio turns. Another interesting application is the enhancement of accuracy of an angle sensor in combination with a pole wheel. Here the pole wheel has to be adapted to the number N of turns the combination of loops is able to count. If the angle sensor gets an accuracy of say 1°, the accuracy the combined system offers is $1/N°$ opening a wide range of application where expensive high accurate angle detectors can be substituted by a much cheaper combination of a low-price magnetic angle sensor and a turn counter.

As discussed above the use of the domain wall based counters with a loop geometry needs a predefined starting configuration (definition of number and position of at least one domain wall per loop). The erase of unwanted domain walls by pinning it by using local magnetic fields generated by electrical conduits is described in detail in [37].

4.5. Physics of the moving domain walls

To get a deeper insight in the functionality of domain wall based devices we have to discuss the dynamics of the movement of 180° domain walls in more detail. The geometry of the domain wall conduit consists of straight lines of about 100 μm length and half circles or quarters with radii between few and 10 μm and, in the case of closed loops with cusps. The magnetic field responsible for domain wall movement rotates and the domain wall(s) follows this rotation with a distinct lag due to hysteresis. Therefore in the straight lines the domain walls move with a mean velocity in the order of 100–1000 m s^{-1} (see figure 26) resulting in traveling times of 1 to 10 μs for 100 μm lengths. It changes completely after reaching the curved part of the conduit. Here the domain wall moves step by step through the curved part of the spiral or loop. The individual moving distance along the rounded edges depends primarily on the radius and is in general much below 1 μm. Within this condition the kind of moving domain wall depends only on the relation of thickness and width of the conduit the domain wall moves in. As shown in [40] for a thin and small nanowire a transversal domain wall exists and moves through this curvature. With increasing width and thickness of the magnetic conduit the domain wall changes its equilibrium structure for $H = 0$. The transverse wall gets more asymmetric forming an asymmetric transverse domain wall and further on a vortex or antivortex wall is formed. This wall moves within the curved part of the conduit small steps

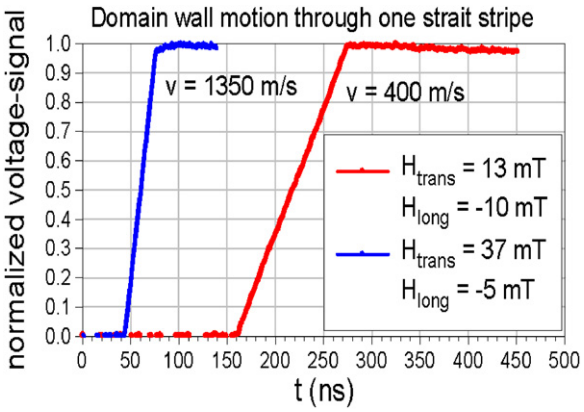

Figure 26. Examples of domain wall movement under different conditions along a straight 40 μm line.

until the driving force, here the longitudinal component of the magnetic field, gets below the minimum field necessary for a continuous movement. The domain wall movement is much more complicated in the straight lines. Here the kind of domain wall depends not only on the cross section of the conduit but also on the kinetics. As proposed by Walker [41] the state of the domain wall changes in a periodic way leading to a stop and go of the domain walls [42, 43].

With respect to application we have to consider two aspects directly connected with sensor parameters: first, the typical mean velocity v_{mean}, a domain wall can achieve through a straight line, is of the order of some 100 m s^{-1}. Therefore the maximum rotational speed is directly related to the length l_{crit} of the straight lines. As a rough estimation the angle rotation causing an angle lag between the direction of the rotating magnetic field and the equilibrium position of the domain wall must be below $p/2$ in every case. Therefore it should not be larger than $l_{\mathrm{crit}}/v_{\mathrm{mean}}$ times 1/8. For $l = 100$ μm the critical frequency is of the order of 100 kHz. An increase of the maximum rotational speed to 1 MHz is possible only by using TMR stacks allowing for lateral extensions of any loop or spiral below 10 μm.

Second, the important device limiting parameter is the magnetic window, in which the sensor works error free. Below a minimum magnetic field the pinning due to roughness or other magnetic disturbances cannot be avoided under every possible condition. The transition from 100% error rate to zero occurs within a comparably broad transition as displayed in figure 27. This is a direct result of the stochasticity of the domain wall movement and the local geometrical parameters such as edge roughness, interface roughness mediated interlayer coupling variation and thickness fluctuation. As shown in [44] any thickness fluctuation acts as a comparably strong pinning site for the vortex core of the domain wall.

On the other hand there exists a field H_{max} at which the rotating field itself is able to create domains and therefore additional new and unwanted domain walls are generated outside the domain wall generator in the case of the spiral or within closed loops. Because this process generates erroneous counting, any field strength larger than this value has to be avoided under all conditions by suitable design of the whole system. The value H_{max} is determined by geometric and

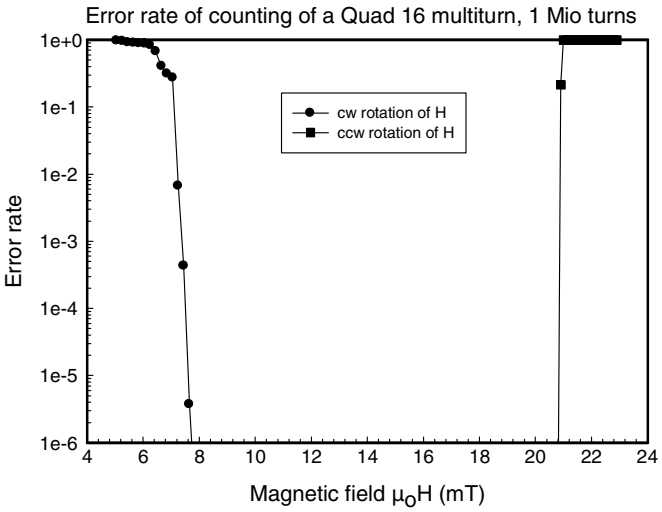

Figure 27. Dependence of the counting error rate of a Quad16 multiturn from the strength of the rotating magnetic field.

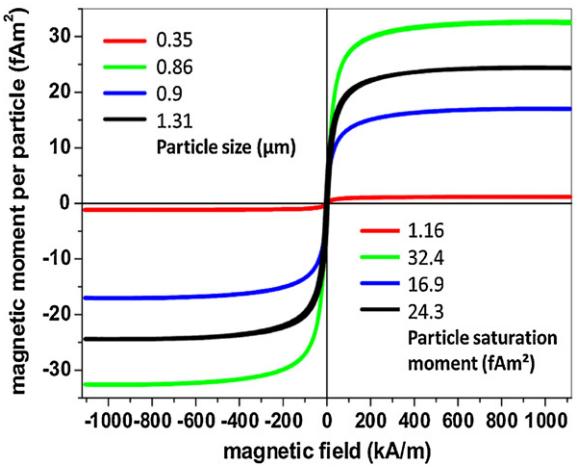

Figure 28. Picture of the magnetic moment of typical magnetic markers as a function of the external magnetic field. The differences are due to different filling factors with magnetic material (see [51] and references therein).

magnetic properties and can be estimated to $H_{\max} \sim d/2w^{*}M_s$ where d and w are the thickness and width, respectively, and M_s the saturation magnetization of the magnetic conduit. As a result the transition from 100% error to error-free working is very sharp (within 0.2 mT). Therefore by using an appropriate geometry, the limiting parameter can be adapted. In a first approximation the device related ratio $H_{\min}/H_{\max}$ is around 0.4 in our GMR stacks.

To guarantee the error-free sensing over the lifetime, the sensor must be tested by millions of different domain wall movements because of the stochasticity of this process. Therefore for the determination of the magnetic window, the number of domain wall movements for testing should be comparable to the number of the movements expected within the lifetime of the products, at least of some millions. Examples for the error rate in dependence of the rotating field strength are shown in figure 27. Every field value was tested for 8 million of domain wall movements, and within the window of 7.8 mT$<$ B $<$ 20.4 mT no error occurs.

5. Magnetoresistive sensors for biotechnology

MR or magnetic biosensors use a new detection method for molecular recognition reactions based on two sensor technologies: GMR or TMR. These sensors are used to detect the presence of magnetic particles which are specifically attached to the biological target molecules [45]. The magnetic stray field of these particles is picked up by an MR sensor as a change of the electrical resistance, and the sensor is usually embedded in a microfluidic environment. Compared to, e.g., detection methods using fluorescent markers [46], magnetic biosensors have a number of advantages, including low background signal from the environment, low molecular detection limits, flexibility and the direct availability of an electronic signal suitable for further automated analysis. This makes them a promising choice for the use single biochips or even in lab-on-a-chip systems.

Both measurement techniques using GMR- or TMR-sensors are presented here. Different configurations are discussed and the results for GMR sensors are compared to an analysis of the same biological systems marked with fluorescence dyes. Down to a concentration of about 10 pg μl^{-1} of, e.g., DNA molecules the MR technique is competitive with present standard analysis methods. The capability of the TMR sensors to detect even nano-sized markers is additionally pointed out.

5.1. Magnetic markers

The magnetic carriers (often called beads) usually detected by the sensors consist of small superparamagnetic particles embedded in a polymer matrix. The total sizes range from some μm down to about 100 nm. These composite particles are linked to, e.g., DNA or proteins (often by an avidin–biotin bond) and thereby enable highly specific detection of complementary molecules.

The most commonly used markers in biomedicine are based on magnetite (Fe_3O_4) or maghemite (Fe_2O_3). Their magnetic properties and biocompatibility has been extensively investigated; they can be metabolized by the human body (through liver and kidneys). Nowadays, they are also used as contrast agents in MRI techniques or as hyperthermia agents in cancer therapies [47]. Further applications for micro- or nanoparticles are foreseen in drug delivery systems to specific locations of disease, magnetic cell separation, biomolecular technology [48] and single cell experiments [49]. Their functionalization with biomolecules is mandatory for the use in biomedicine, but due to different biological treatments, their magnetic moment can be reduced as compared to the magnetic bulk material [50]. Because the properties of these particles are determining the required sensor characteristic, figure 28 shows a typical magnetization curve. The particles exhibit a superparamagnetic behavior and saturation is approached within 10% at fields (H) above 300 kA m^{-1}. Nevertheless, a substantial magnetic moment can be induced already

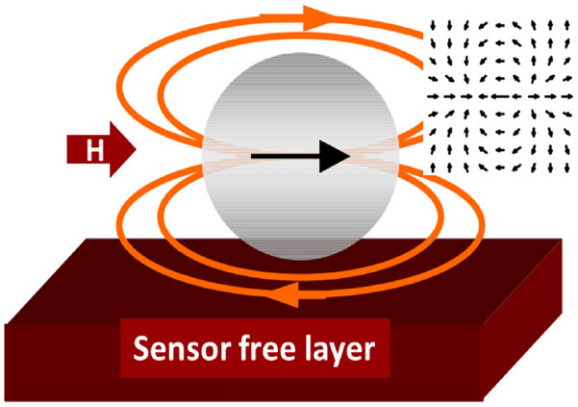

Figure 29. Picture of a magnetic particle on top of a sensor with a stray field induced by an external in-plane magnetic field H. The in-plane components of the stray field in the sensor's free layer are sketched in the inset.

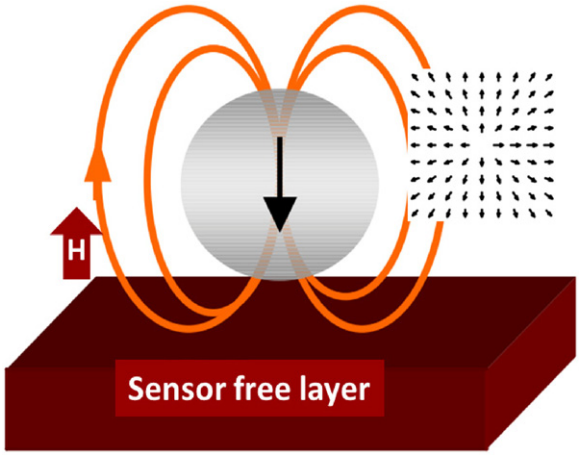

Figure 30. A magnetic particle on top of a sensor with a stray field induced by an external perpendicular magnetic field H. The in-plane components of the stray field in the sensor's free layer are sketched in the inset.

with much smaller fields. Typical measurement setups use maximum field strengths of some 10 kA m^{-1}, where the magnetic moment M can be described by a linear relation $M \sim \chi H$.

Although for established measurement methods, such as techniques using fluorescence, the environment often causes a large background signal, there are usually negligible magnetic signals from the microfluidic environment as well as from biological systems. Thus the use of magnetic markers has the potential to detect extremely small quantities of the particles. Moreover, the magnetic particles offer an additional feature: they can be manipulated on chip via currents running through specially designed line patterns. This enables either a concentration of particles at the location of the sensor or the transport as well if ac magnetic fields are used.

5.2. Sensors for detecting biomolecules

For the application in biotechnology, the small magnetic particles discussed in the foregoing section which are linked to biomolecules must be detected. This can be done either statically with a particle situated on top of a sensor, or dynamically with a fluid carrying the particles [51].

For the detection of small magnetic particles situated above a magnetic sensor, some special requirements are necessary. The situation is illustrated in figures 29 and 30.

In general, typical sensors are only sensitive to magnetic field components which are in the plane of the sensor's free layer. In the MR biosensors discussed in this section, these field components are induced by the stray field of the magnetic particle which in turn is induced by an external magnetic field H of the order of some 10 kA m^{-1}. Due to a relatively small susceptibility of the particles in the range of some percent [52] the magnitude of this stray field is smaller than about 1 kA m^{-1}. Thus the measurement technique illustrated in figure 30 (perpendicular field) is often preferred because the external field in this arrangement does not influence the response of the sensor. Careful arrangement of the setup, however, is necessary to avoid any in-plane components of the external field H (see figure 30). For such proper measurement setup, the field components which have to be detected are of the order of few tenths of a kA m^{-1} provided the distance between particle and sensor is small and their spatial extent is restricted to an area of about 1 μm $\times$ 1 μm given a particle with a radius of around 1μm. Thus the sensitivity and the signal-to-noise ratio of the sensor have to be large to supply reliable measurement results. In practice, a sensitivity of at least 1% resistance change per 1 kA m^{-1} applied field, a field range of an ideally linear sensor response of about 10 kA m^{-1} and a signal-to-noise ratio larger than 2 are required.

5.3. GMR: sensing of particles

If one screens the available sensors for these purposes, either spin valve type GMR-trilayers similar as those used in hard disk read heads or antiferromagnetically coupled GMR-multilayers seem most appropriate. In both types of sensors, the sensitivity can be tuned by either varying the material of the sense layer (spin valve) or by tuning the strength of the antiferromagnetic coupling and the magnetic layers (multilayers). In particular for multilayers made from Permalloy ($Ni_{80}Fe_{20}$) and Cu in the second antiferromagnetic coupling maximum (film system: $Si/(Ni_{80}Fe_{20})_{1.6\ nm}/(Cu_{1.9\ nm}/(Ni_{80}Fe_{20})_{1.6\ nm}]_{10}/Ta_{3nm}$) the GMR can be tuned to be highly sensitive and nearly free of hysteresis as shown in figure 28 for a spiral type multilayer-sensor.

For the realization of a MR sensing device for small magnetic particles the absolute value of the device resistance is not the appropriate signal due to the scatter of the individual resistances of different sensors and the temperature dependence of the GMR (and TMR) as discussed in the foregoing sections. The signal needed, however, is only the change of resistance upon coverage of the sensor with particles. Thus a reference can be used which is kept at the same temperature as the measured sensor and remains uncovered as illustrated in figure 32.

By comparing the resistances of the two sensors, a highly sensitive detection of particles becomes possible. Figure 33

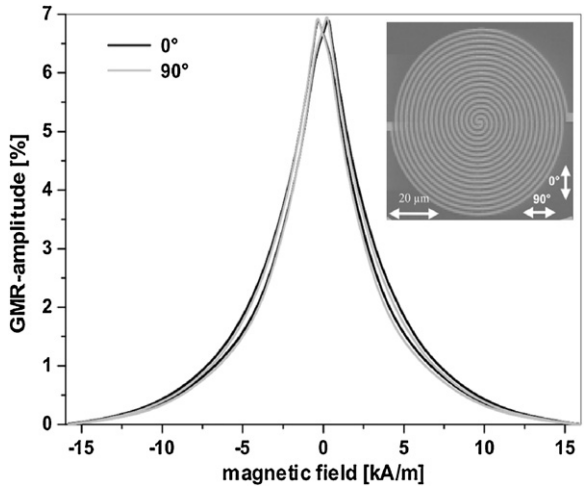

Figure 31. MR response of a spiral-shaped sensor element to in-plane magnetic fields. The inset shows an SEM picture of the sensor used for this measurement. The response is highly isotropic due to the sensor shape and the low anisotropy of Permalloy.

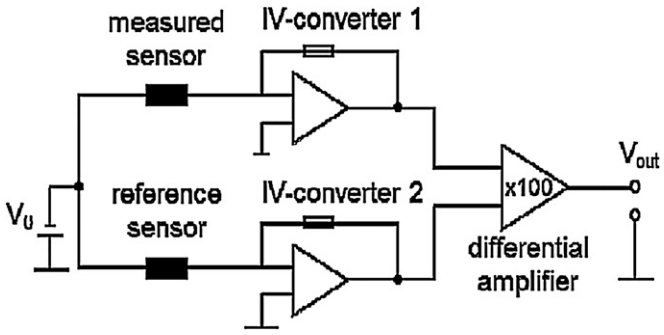

Figure 32. Circuitry for detecting magnetic particles with MR sensors: the currents running through the reference sensor and the measured sensor are compared and the difference of these signals is amplified to form the output voltage.

shows the output signal from the circuit of figure 32 if a spiral type GMR sensor (Permalloy/copper multilayer) is used for detection. A clear signal caused by the coverage of the sensor with magnetic particles can be obtained. In this example, 5% of the sensor surface was covered with magnetic particles (inset of figure 31). For a typical magnetic field of 15 kA m^{-1}, an output voltage of around 50 mV can be realized for this degree of coverage, whereas the control experiment (uncovered sensor) shows only noise in the range of some mV.

From these measurements it becomes clear, that the use of highly sensitive MR sensors is a promising tool to detect magnetic particles bound to target molecules. For estimating the potential of this method, however, a comparison with established standard methods is necessary.

5.4. Comparison to standard methods and detection limits

Important questions in this respect are the biological sensitivity to small amounts of DNA and the dynamic range of the sensor, i.e. the difference in DNA concentration between a minimum detectable signal and saturation of the sensor. To compare the

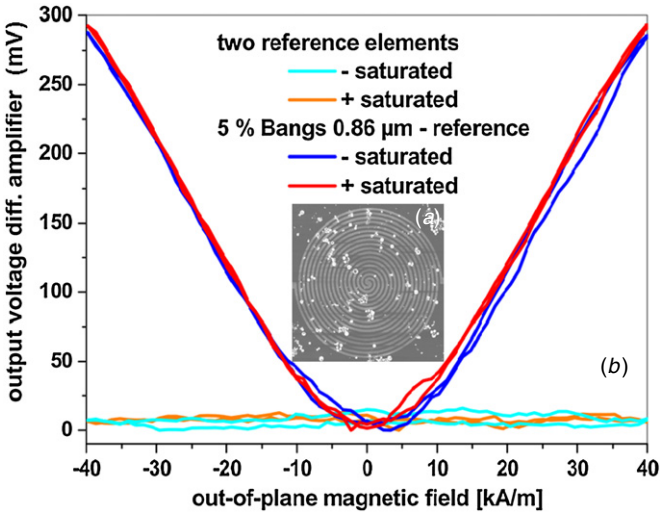

Figure 33. The output voltage of a sensor chip with magnetic particles on top (SEM image shown in the inset). The coverage was 5% of the sensor area.

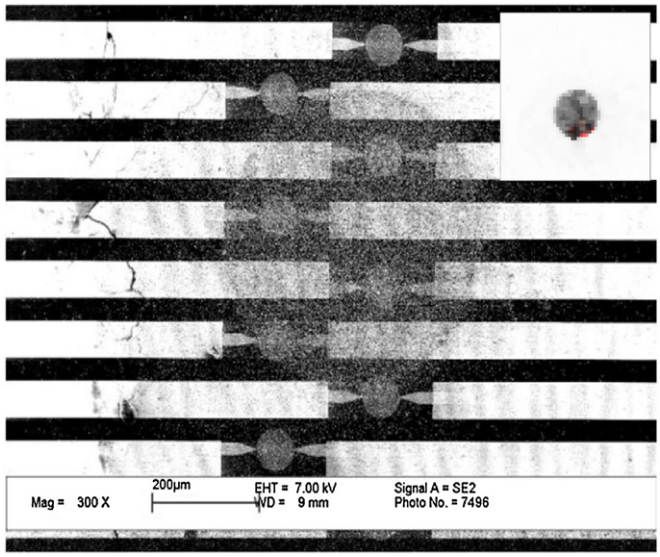

Figure 34. An array of spiral type GMR sensors covered by a spot of 1 kB DNA (1000 bases) bound to magnetic markers. The DNA was also marked with fluorescent dyes (Cy3). The inset shows the fluorescence signal from this spot which was used for the comparison to the GMR-based signal.

results, the concentrations have to be calibrated by a standard method. Here, fluorescent markers (Cy3 streptavidin) have been used. To ensure a meaningful comparison, both the MR sensor and the fluorescent chip have been treated as identical as possible. Figure 34 shows a sensor array covered with magnetic particles attached to a 1kB DNA segment which was specifically bound to the sensor surface by a complementary DNA strand [54].

In order to compare the data from the MR biosensor to the fluorescent detection method, the average signals of each probe DNA concentration are normalized to the average signal of the unspecific probe DNA sensor elements. Along with the data from the fluorescent chip and the corresponding

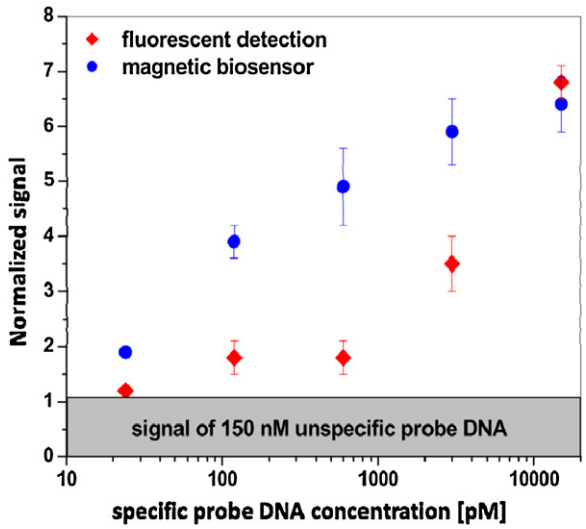

Figure 35. Comparison of the normalized signals of MR biosensors with fluorescence techniques in dependence of the concentration of 1 kB DNA. The lower bound (gray shaded area) is defined by the signal produced by a 150 nM unspecific probe DNA.

standard deviations, those normalized signals are plotted over the corresponding probe DNA concentration in figure 35.

Apparently, both methods are sensitive to the whole range of probe DNA concentration, ranging from 16 pg μl^{-1} to 10 ng μl^{-1}, i.e. almost over a range of three orders of magnitude. At the high concentration region, both sensor types are saturated, whereas the sensitivity at the lower end is limited by unspecific signals. However, in the case of the magnetic biosensor, the density of bound markers within unspecific probe DNA spots is the same as in regions outside of the DNA spots. Contrary to that, there is some additional background signal within the unspecific probe DNA spots in the case of fluorescent detection, which decreases the relative sensitivity. Therefore, in this experiment the sensitivity of the magnetic biosensor is superior to fluorescent detection at low probe DNA concentrations, for example by a factor of 2.7 at 600 pg μl^{-1}.

5.5. Comparison between GMR and TMR sensors

Because the signal obtained from TMR sensors can be much larger than that from GMR devices, TMR promises to increase the sensitivity of MR biosensors even further. While the technical setup is very similar to GMR in particular, the patterning processes are more complicated due to the need for an upper contact of the TMR cell. This also increases the distance between the magnetic particles and the free layer in the sensor. Nevertheless, as shown in figure 36, the signal obtained from a TMR sensor is larger only by a factor of 4 as compared to GMR.

An additional issue is the noise in TMR junctions. Because their resistance is usually larger as compared with GMR devices, the corresponding noise is increased subsequently. In application, using TMR sensors in biochips hinders the moment because the noise has to be eliminated by a long measuring period. Work to avoid this issue is, however, in progress and promising results have been obtained for single crystalline sensor devices which exhibit excellent TMR combined with low noise.

6. Summary

MR effects represent basically the change of a metal system's electric resistivity under the influence of an external magnetic field. There are many configurations possible, depending on the materials used, the functioning principle and the intensity of the effect. In 1988, Grünberg [3] and Fert [4], with their respective teams discovered the ground breaking GMR effect and showed that it was possible to generate resistance changes of 10% to 50% and sensitivities of about 20 mV (VmT)$^{-1}$. Since 1988 many different types of GMR-sensors, such as multilayer sensors or spin valve sensors for applications like read sensors for hard drives, angle sensors, multiturn angle sensors, electrical current measurement or linear position measurement as well as the detection of biomolecules, have been developed. During the last decade GMR technology led to particularly large advances in the fields of biosensing, multiturn angle sensing and electrical current sensing.

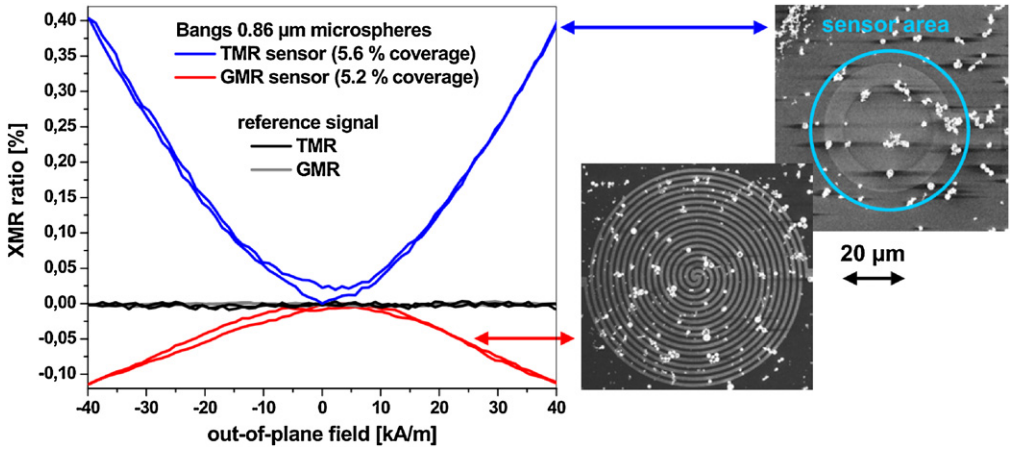

Figure 36. Comparison of the response of TMR and GMR type sensor elements to an approximately equal surface coverage of Bangs 0.86 μm magnetic particle.

Research on GMR spin valve sensor technology resulted in an extremely low hysteresis which is the foundation for the application in accurate measurement systems such as [31] current sensors. For galvanically isolated and therefore safe and reliable current measurement, GMR technology based sensor can at once offer a high accurate and large bandwidth. But to exploit the outstanding possibilities the whole measurement system should consist of GMR sensors arranged in a special Wheatstone configuration on a u-shaped conductor to enable differential measurement and electronic advanced circuitry including high quality digital signal conditioning [29]. The lowest measurement errors of about 0.25% in a temperature range from −10 °C to 70 °C has achieved digital signal conditioning based on B-spline interpolations [31]. That method usually used in the fields of digital image processing comes with enormous flexibility in combination with low mathematical complexity and is therefore best suited for compact, low-cost digital hardware such as FPGAs or DSPs.

Besides high-quality GMR spin valve sensors for accurate current sensing, the new class of magnetic multiturn sensors, using the dedicated geometries of magnetic nanowires, has been developed during the last few years. These nanowires allow the storage of magnetic configurations which changes half turn-by-half turn by domain wall motion. Low-number counters use a spiral-like nanowire connected with a domain wall generator, which injects 180° domain walls every half turn. Closed loops, each one able to count a number of turns prime to the number of all other loops use a constant number of domain walls moving within the closed loops. This kind of GMR sensor allows us to count a maximum number of turns >100 up to >10 million depending on the number of loops in use. This novel sensor allows us to count turns even without voltage supply thus gaining a big safety advantage in many applications.

For magnetic biosensors, the goal of quantitative molecule detection corresponds to the requirement of resolving the presence of magnetic markers within a given dynamic range. Single molecule detection can be accomplished by shrinking the size of the sensor to the dimensions of the relevant labels [55], i.e. to the sub-μm size scale. In this regime, it becomes increasingly demanding to build GMR type sensors with sufficient resistivity to allow an easy readout of the signals, which is due to the highly conductive all-metallic structure of this sensor type and the resulting low resistance. Contrarily, the resistances of TMR type sensors increases with decreasing area of the tunneling cell, and elements with a resistance in the kΩ range have been demonstrated at sub-100 nm length scales for MRAM applications [56]. For the major part of applications, however, single marker detection is not in the focus. An ideal type of magnetic biosensor would consist of an array of GMR sensor elements which give an output signal, depending linearly on the number of magnetic markers on the sensor surface. For these applications, the integration of such sensors in microfluidic systems providing molecule inlet, marker-binding, sensing and waste disposal is currently developed. Combined with on-chip-manipulation of markers and molecules via ratchet transport or magnetic gradient fields such systems offer very promising pathways towards handheld systems for point of care diagnostics. This research is at present in the focus of many groups worldwide [57–59].

Acknowledgment

RM acknowledges the financial support by the German Ministry of Education and Research under grant no 13N 10125.

References

[1] Thomson W 1856 On the electro-dynamic qualities of metals: effects of magnetization on the electric conductivity of nickel and of iron *Proc. R. Soc. Lond.* **8** 546–50
[2] Nickel J 1995 Magnetoresistance overview *HP Labs Technical Reports* HPL-95-60 pp 1–11
[3] Binasch G, Grünberg P, Saurenbach F and Zinn W 1989 Enhanced magnetoresistance in layered magnetic structures with antiferromagnetic interlayer exchange *Phys. Rev.* B **39** 4828–30
[4] Baibich M N, Broto J M, Fert A, Nguyen van Dau F, Petroff F, Eitenne P, Creuzet G, Friederich A and Chazelas J 1988 Giant magnetoresistance of (0 0 1) Fe/(0 0 1)Cr magnetic superlattices *Phys. Rev. Lett.* **61** 2472–5
[5] Nobelprize.org 2012 *The Nobel Prize in Physics 2007* www.nobelprize.org/nobel_prizes/physics/laureates/2007
[6] Parkin S S P, More N and Roche K P 1990 Oscillations in exchange coupling and magnetoresistance in metallic superlattice structures: Co/Ru, Co/Cr, and Fe/Cr *Phys. Rev. Lett.* **64** 2304–07
[7] Fert A 2008 The present and the future of spintronics *Thin Solid Films* **517** 2–5
[8] Tumanski S 2001 *Thin Film Magnetoresistive Sensors* (Bristol: Institute of Physics Publishing)
[9] Treutler C P O 2001 Magnetic sensor for automotive applications *Sensors Actuators* A **91** 2–6
[10] Rieger G, Ludwig K, Hauch J and Clemens W 2001 GMR sensors for contactless position sensing *Sensors Actuators* A **91** 7–11
[11] Mahdi A E, Panina L and Mapps C 2003 Some new horizons in magnetic sensing—high-Tc SQUIDs, GMR and GMI materials *Sensors Actuators* A **105** 271–85
[12] Stork T Electronic compass design using KMZ51 and KMZ52 Application Note: Philips Semiconductors Systems Laboratory, Hamburg, Germany
[13] von Helmolt R, Wecker J, Holzapfel B, Schultz L and Samwer K 1993 Giant negative magnetoresistance in perovskite like $La_{2/3}Ba_{1/3}MnOx$ ferromagnetic films *Phys. Rev. Lett.* **71** 2331
[14] Ramirez A P 1997 Colossal magnetoresistance *J. Phys.: Condens. Matter* **9** 8171–99
[15] Phan M and Peng H 2008 Giant magnetoimpedance materials: fundamentals and applications *Prog. Mater. Sci.* **53** 323–420
[16] Niedermeier U, Vieth M, Pätzold R, Sarfert W and von Seggern H 2008 Enhancement of organic magnetoresistance by electrical conditioning *Appl. Phys. Lett.* **92** 193309
[17] Vouille C, Fert A, Barthélémy A, Hsu S Y, Loloee R and Schroeder P A 1997 Inverse CPP-GMR in (A/Cu/Co/Cu) multilayers (A = NiCr, FeCr, FeV) and discussion of the spin asymmetry induced by impurities *J. Appl. Phys.* **81** 4573

[18] Mott N F 1936 The electrical conductivity of transition metals *Proc. R. Soc. Lond.* A **153** 699

[19] Tsymbal E Y and Pettifor D G 2001 Perspectives of giant magnetoresistance *Solid State Phys.* **56** 113–237

[20] Wolf S A, Awschalom D D, Buhrman R A, Daughton J M, von Molnár S, M Roukes M L, Chtchelkanova A Y and Treger D M 2001 Spintronics: a spin-based electronics vision for the future *Science* **294** 1488–95

[21] Parkin S S P, Bhadra R and Roche K P 1991 Oscillatory magnetic exchange coupling through thin copper layers *Phys. Rev. Lett.* **66** 2152–5

[22] Liu K, Nagodawithana K, Searson P C and Chien C L 1995 Perpendicular giant magnetoresistance of multilayered Co/Cu nanowires *Phys. Rev.* B **51** 7381

[23] Barthelemya A *et al* 2002 Magnetoresistance and spin electronics *J. Magn. Magn. Mater.* **242–245** 68–76

[24] Zabel H 2009 Progress in spintronics *Superlatt. Microstruct.* **46** 541–53

[25] Beltran H, Reig C, Fuster V, Ramirez D and Cubells-Beltran M D 2007 Modeling of magnetoresistive-based electrical current sensors: a technological approach *IEEE Sensors J.* **7** 1532–7

[26] Ripka P 2010 Electrical current sensors: a review *Meas. Sci Technol.* **21** 112001

[27] Pannetier-Lecoeur M, Fermon C, de Vismes A, Kerr E and Vieux-Rochaz L 2007 Low noise magnetoresistive sensor for current measurement and compasses *J. Magn. Magn. Mater.* **316** e246–48

[28] NVE 2012 AAV003-10E Current Sensor www.nve.com/webstore/catalog/product_info.php?cPath=27_28&products_id=544 *Last accessed July 2012*

[29] Jedlicska I, Weiss R and Weigel R 2008 Improving GMR current sensor measurements through hysteresis modeling *IEEE Power Electronics Specialists Conf. (Rhodes, 15–19 June)* pp 4781–5

[30] Jedlicska I, Weiss R and Weigel R 2010 Linearizing the output characteristic of GMR current sensors through hysteresis modeling *IEEE Trans. Ind. Electron.* **57** 1728–34

[31] Bluemm C, Weiss R and Weigel R 2010 Correcting nonlinearity and temperature influence of sensors through B-spline modeling *IEEE Int. Symp. on Industrial Electronics (Bari, 4–7 July)* pp 3356–61

[32] Weiss R, Behringer K, Bluemm C and Weigel R 2010 Precision current sensor with exceptional large bandwidth *Bodo's Power Syst.* **10** 32–4

[33] Diegel M *et al* 2004 360° domain wall investigation for sensor applications *IEEE Trans. Magn.* **40** 2655–7

[34] Geng L W D and Jin Y M M 2012 Generation and storage of 360 degrees domain walls in planar magnetic nanowire *J. Appl. Phys.* **112** 083903

[35] Diegel M, Mattheis R and Halder E 2005 Multiturn counter using movement and storage of 180 degrees magnetic domain walls *Sensor Lett.* **5** 118–22

[36] Diegel M, Glathe S, Mattheis R, Scherzinger M and Halder E 2009 A new four bit magnetic domain wall based multiturn counter *IEEE Trans. Magn.* **45** 3792

[37] Mattheis R, Glathe S, Diegel M and Hübner U 2012 Concepts and steps for the realization of a new domain wall based giant magnetoresistance nanowire device: from the available 2^4 multiturn counter to a 2^{12} turn counter *J. Appl. Phys.* **111** 113920

[38] Allwood D A, Xiong G, Cooke M D, Faulkner C C, Atkinson D, Vernier N and Cowburn R P 2002 Submicrometer ferromagnetic NOT gate and shift register *Science* **296** 2003

[39] Allwood D A, Xiong G, Faulkner C C, Atkinson D, Petit D and Cowburn R P 2005 Magnetic domain-wall logic *Science* **309** 1688

[40] Thiaville A and Nakatani Y 2006 *Spin dynamics in confined magnetic structures III* ed B Hillerbrands and A Thiaville (New York: Springer) p 161

[41] Schryer N L and Walker L R 1974 The motion of 180° domain walls in uniform dc magnetic fields *J. Appl. Phys.* **45** 5406

[42] Beach G S D, Nistor C, Knutson C, Tsoi M and Erskine J L 2005 Dynamics of field-driven domain-wall propagation in ferromagnetic nanowires *Nat. Mater.* **4** 741

[43] Glathe S, Mattheis R and Berkov D V 2008 Direct observation and control of the Walker breakdown process during a field driven domain wall motion *Appl. Phys. Lett.* **93** 072508

[44] Chen T Y, Erickson M J, Crowell P A and Leighton C 2012 Surface roughness dominated pinning mechanism of magnetic vortices in soft ferromagnetic films *Phys. Rev. Lett.* **109** 097202

[45] Baselt D R, Lee G U, Natesan M, Metzger S W, Sheehan P E and Colton R J 1998 A biosensor based on magnetoresistance technology *Biosens. Bioelectron.* **13** 731

[46] Goldys E M 2009 *Fluorescence Applications in Biotechnology and Life Sciences* (New York: Wiley)

[47] Reiss G and Hütten A 2005 Magnetic nanoparticles—applications beyond data storage *Nat. Mater.* **4** 725

[48] Hoet P H M, Brüske-Hohfeld I and Salata O V 2004 Nanoparticles—known and unknown health risks *J. Biotechnol.* **2** 12

[49] Shoshi A *et al* 2012 Magnetoresistive-based real-time cell phagocytosis monitoring *Biosens. Bioelectron.* **36** 116

[50] Buschow K H J 2006 *Handbook of Magnetic Materials* vol 16 (Amsterdam: Elsevier)

[51] Reiss G *et al* 2005 Magnetoresistive sensors and magnetic nanoparticles for biotechnology *J. Mater. Res.* **20** 3294

[52] Bor Fuh C, Lai M H, Lin L Y and Yeh S Y 2000 A method for determination of particle magnetic susceptibility with analytical magnetapheresis *Anal. Chem.* **72** 3590

[53] Weddemann A, Auge A, Albon C, Wittbracht F and Hütten A 2009 On the resolution limits of tunnel magnetoresistance sensors for particle detection *New J. Phys.* **11** 113027

[54] Schotter J, Kamp P B, Becker A, Pühler A, Reiss G and Brückl H 2004 Comparison of a prototype magnetoresistive biosensor to standard fluorescent DNA detection *Biosens. Bioelectron.* **19** 1149

[55] Tondra M, Porter M and Lipert R J 1999 Model for detection of immobilized superparamagnetic nanosphere assays labels using giant magnetoresistive sensors *J. Vac. Sci. Technol.* A **18** 1125

[56] Yoshida C, Ochiai T, Iba Y, Yamazaki Y, Tsunoda K, Takahashi A and Sugii T 2012 Demonstration of non-volatile working memory through interface engineering in STT-MRAM *2012 Symp. on VLSI Technology Digest of Technical Papers* p 59

[57] Haun J B, Yoon T-J, Lee H and Weissleder R 2010 Magnetic nanoparticle biosensors *Wiley Interdiscip. Rev. Nanomed. Nanobiotechnol.* **2** 291–304

[58] Silva D C F, Azevedo A M, Fernandes P, Chu V, Conde J P and Aires-Barros M R 2012 Design of a microfluidic platform for monoclonal antibody extraction using an aqueous two-phase system *J. Chromatogr.* A **1249** 1

[59] Gaster R S, Xu L, Han S-J, Wilson R J, Hall D A, Osterfeld S J, Yu H and Wang S X 2011 Quantification of protein interactions and solution transport using high-density GMR sensor arrays *Nat. Nanotechnol.* **6** 314

QUERIES

Page 1

Q1

Author: Please be aware that the color figures in this article will only appear in color in the Web version. If you require color in the printed journal and have not previously arranged it, please contact the Production Editor now.

Q2

Author: Please check the paper carefully (to ensure that your intended meaning is unaffected) as more than the usual number of changes have been made.

Page 7

Q3

Author: Please check that figures 14 and 31 are not appearing in sequential order in the text.

Page 9

Q4

Please check the sentence starting: 'This wall was transported a half turn . . . ' for sense.

Q5

Author: Please check for the correctness of figure 2D in the sentence starting: 'The counting of a low . . . '.

Page 10

Q6

Author: Please check the given reference number [364], replace this with correct reference number(s).

Page 16

Q7

Author: Please check the details for any journal references that do not have a blue link as they may contain some incorrect information. Pale purple links are used for references to arXiv e-prints.

Q8

Author: Please update/provide more information in reference [12], if possible.

Page 17

Q9

Author: Please check that references [36] and [53] are not cited in the text.